

Original Article

Improved Grid Stability Optimisation and Fault Detection in PV +EV Integrated Systems with Partial Shade Using NCNN-EGSA Optimization Techniques

S. Venkata Ramudu Naik¹, Pulivarthi Nageswara Rao²

^{1,2}Department of Electrical Electronics and Communication Engineering, GITAM School of Technology, Gandhi Nagar, Rushikonda, Visakhapatnam, Andhra Pradesh, India.

¹Corresponding Author : vsugali@gitam.in

Received: 17 April 2025

Revised: 18 May 2025

Accepted: 20 June 2025

Published: 27 June 2025

Abstract - The co-utilization of Electric Vehicles (EVs) in photovoltaic (PV)-based distribution networks bridges the opportunities and challenges associated with grid stability and operational reliability, particularly under partial shading conditions. In this study, an improved grid management scheme based on a Novel Convolutional Neural Network (NCNN) was developed and trained using an Enhanced Golden Search Algorithm (EGSA). The proposed system solves two important problems: (1) high-precision fault detection and (2) real-time stability improvement in PV-EV integrated grids. NCNN is designed to learn spatial and temporal information in system parameters such as voltage, current, and power flow. Meanwhile, EGSA can adjust hyperparameters effectively, which promotes model performance and accelerates the convergence rate. Common failures such as line-to-ground and partial shading-induced faults are identified with high sensitivity, and a diagnosis accuracy of 99.51% and a fast response time of 0.5 s are obtained. The simulation results indicate a 25% enhancement in the grid stability and a 12% decrease in energy consumption owing to EV integration. In addition to improving energy efficiency and operational robustness, the framework improves the robustness of the smart grid. These findings confirm that the NCNN-EGSA is an effective and intelligent strategy for future PV-EV distribution systems.

Keywords - Electric Vehicles, Photovoltaic systems, Grid Stability, Fault Detection, Novel Convolutional Neural Network (NCNN), Enhanced Golden Search Algorithm (EGSA), Partial Shading, Fault Classification.

1. Introduction

The rapid and significant increase in photovoltaic (PV) systems and Electric Vehicles (EVs) in today's power distribution systems creates significant problems for the stability of traditional grids. With both technologies emerging as keys for the transition to decentralized and decarbonized power systems, they inherently bring dynamic operating scenarios, including partial shading, fast-changing solar irradiance, bidirectional power flow, and non-uniform EV charging load patterns [1, 2]. Such variations in power quality may cause an interruption of voltage regulation and deviation from frequency, and the voltage level may become increasingly challenging to maintain, most notably under real-time conditions. Machine Learning (ML) and Deep Learning (DL) have emerged as promising techniques for providing intelligent data understanding and system-level decision-making. These techniques have been shown to successfully perform tasks such as fault type identification, load prediction, renewable energy forecasting, and grid state estimation and monitoring [3, 4]. However, some problems could make it challenging to connect PV-EV to the grid, such as Power Quality Disturbances (PQDs) and issues with detecting and classifying faults, including line-to-ground short circuits and string mismatches caused by changes in

sunlight. If not rectified effectively, such conditions may significantly reduce the secondary energy delivery efficiency and endanger safe and reliable operation [5, 6]. Conventional fault detection strategies, such as rule-based, model-based and statistical-based strategies, will not be able to meet the nonlinear and multivariable nature of the renewable-based microgrid. They may be stiff and expensive to compute and cannot adapt to changing environments in real-time [7, 8]. Conversely, data-driven models, particularly those based on CNN, present a more effective learning framework for exploiting the spatial-temporal correlations and underlying patterns of the system's electrical response [9, 10]. Recent research has highlighted the worthiness of deep structures such as LSTMs [6], stacks of ensemble models [8], and hybrid CNNs [13] for accurate fault diagnosis across diverse PV system scenarios.

Furthermore, more advanced metaheuristic optimization methods, such as Lyrebird Optimizer, Energy Valley Optimiser, and golden search-based algorithms, have been incorporated to improve hyperparameter tuning, training convergence, and model generalization in fault-detection networks [3, 13, 19]. This study extends this research by introducing an innovative New Convolutional Neural Network (NCNN) model incorporated into the Grid



Optimization And Fault Detection Model (GO-FDM). The optimization rule is formulated using EGSA, which can adjust the pivotal parameters adaptively to the convergence rate and deep learning. The hybrid NCNN-EGSA system was developed to achieve the dual goals of (1) high accuracy (low latency) fault detection in PV–EV driven distribution networks and (2) real-time grid stability optimization under the changing thrust of solar power and EV demand. In contrast to traditional CNN models, the proposed NCNN contains multi-scale feature extraction, a channel attention module, and customized loss. This representation is instrumental in furthering the ability to learn effectively from complex system signals without needing fixed-scale features or exhaustive pre-processing.

The performance was demonstrated on a 100 kW grid-connected PV array benchmark dataset on a 25 kV distribution feeder with real-time sensor data, thermographic images and simulated faults. Experimental results confirm the superiority of the proposed NCNN-EGSA model, as they contribute to a 25% increase in the stability of the grid voltage/frequency, a 12% decrease in the energy of EV consumption, and a 99.51% detection rate of the fault rate compared to conventional methods such as SVM, KNN, and DT classifiers. These results indicate that the NCNN-EGSA is a scalable, efficient, and innovative approach for tackling the complexity of PV–EV integrated smart grids. It provides a solid basis for in situ grid monitoring, adaptive fault tolerance, and online operational control in a fast-changing energy landscape.

The introduction section carefully points to the research gap and the problem statement. “Some fault detection methods in existing PV–EV integrated distribution networks do not work better under certain scenarios, and a modified, intelligent, and optimized deep learning technique seems essential here.” In the modified section, the authors stated the following: Now, the limitations of current traditional fault detection methods in PV EV integrated distribution are discussed, and it is justified that there is an essential need for a novel, intelligent and optimum deep learning-based approach. The updated version is below.

Fast and large-scale penetration of Photovoltaic (PV) systems and Electric Vehicles (EVs) into modern grid distribution networks imposes new uncertainties on grid operators, which could imply grid instability. Although these technologies are essential for implementing decarbonized and decentralized energy systems, their dynamic behaviour is nonlinear and unpredictable, originating dynamic phenomena like partial shading, impulsive modifications of the solar irradiance and bidirectional power injection to the grid [1, 2]. Such problems contribute to the PQDs, voltage disturbances and frequency fluctuations, especially under operation limitations.

1.1. Research Gap

While the use of ML/DL has been ventured into grid monitoring and management [5, 6], existing fault detection is based mainly on rule-based or model-based techniques, which lack adaptability for the nonlinear and time-variant

nature of the PV–EV-based system [5, 6]. These conventional methods do not scale well and struggle to accurately detect localized faults, including ground short circuits and mismatches of fixed position in the presence of fast shifts in the irradiance and/or do not generalize for complex operating conditions. Additionally, current deep learning models, like basic CNN or LSTM models, often struggle to effectively identify complex fault patterns over different scales or train quickly.

1.1.1. Problem Statement

In order to overcome those challenges, this study attempts to establish a new Structural Based Face Recognition (SBFR) methodology, which consists of a New Convolutional Neural Network (NCNN) model incorporated with an Enhanced Golden Search Algorithm (EGSA). The NCNN-EGSA model was created to improve grid fault detection accuracy and real-time stability in a PV–EV integrated network. The fusion model combines multi-scale feature extraction, channel attention, and adaptive optimization, so inadequate pre-processing or futurization is unnecessary for high-quality classification.

1.1.2. Contribution

The solution of (NCNN-EGSA) can be given by a bi-activity solution: The solution ensures reliable fault detection with low latency in the face of real-time PV–EV grid interference. Stable grid voltage and frequency The system remains stable despite dynamic loads and environmental conditions. The system’s performance is tested with a benchmark dataset containing real-time sensor signals and simulated fault data from a 100-kW PV array interconnected to the 25-kV distribution feeder. The outcomes of the research show remarkable improvements: a much better computational performance of the grid (at the rate of about 25% improvement in grid stability and 12% reduction in the amount of EV energy delivered to the grid) and a 99.3% fault detection rate, which is better than that achieved by traditional classifiers, including SVM, KNN, and DT.

1.2. Objectives

- To develop fault diagnostics in PV–EV systems based on a hybrid deep learning model (NCNN) optimized through the Enhanced Golden Search Algorithm (EGSA).
- To improve grid reliability amid partial shading and dynamic EV load variances.
- To mitigate losses and enhance power distribution efficiency by optimally integrating EVs. Use attention-based neural mechanisms to capture important system features and anomalies.
- To quantitatively analyze and compare the performance of different systems based on criteria including detection accuracy, response time, energy efficiency, and stability index.

1.2.1. Problem Statement

With the introduction of rapidly utilized renewable energy and electric vehicles, PV-integrated distribution

systems have become more complicated. Such systems have to deal with high-level challenges such as partial shading, intermittent energy source availability, and the dynamism of EV charging loads. Classical fault detection and grid management methods do not always work because of the nonlinearity and temporal dependencies that characterize such systems. Furthermore, real-time fault diagnosis under changing conditions while preserving the grid stability remains an open issue. Therefore, it is still necessary to develop innovative, adaptable, and optimization-oriented schemes capable of rapidly detecting and isolating faults and maintaining seamless power transference and grid reliability in a PV–EV interconnected grid. This work seeks to overcome these challenges by presenting an NCNN-EGSA-based methodology for integrated deep learning and evolutionary optimization to enhance grid resilience and efficiency.

2. Materials and Methods

Figure 1 shows the proposed flow diagram; the PV array is the primary solar resource supporting the electricity demand for EV charging and the grid. It generates a specific voltage and current signal according to panel surface environmental conditions (clean, dirty, and shaded), requiring real-time monitoring. The EV charger is a dynamic load that consumes electricity from the PV array or grid. Its penetration brings demand uncertainties that may influence the grid’s stability, particularly under high levels of produced power or fault conditions, such as partial shading conditions. The system constantly monitors important electrical attributes, such as voltage changes, current amplitudes, and power flow direction, to handle this complexity. These signals were critical inputs for the NCNN-EGSA framework. Faults, for example, line-to-ground faults and partial shading, are particularly targeted, as they cause voltage imbalance and introduce nonlinear characteristics to the system. A new type of Convolutional Neural Network (NCNN) layer is presented that can understand how these factors change over time and space, allowing it to detect even small changes in the system. In addition, the EGSA adaptively adjusted the model’s

hyperparameters to enhance the classification accuracy, decrease the detection latency, and speed up the convergence. NCNN, The EV charger is a dynamic load that consumes electricity from the PV array or the grid. Its penetration introduces demand uncertainties that may influence the grid’s stability, particularly under high levels of produced power or fault conditions, such as partial shading. The proposed NCNN-EGSA integrates the monitoring of reliability and optimality in the power grid. The fault diagnosis module can recognize various faults with a sensitivity of 99.51% and is operable in real-time. The practical results of the system improve grid stability. The system’s results are as follows: It achieves improved grid stability, better voltage and frequency regulation, load levelling, and smaller variation ranges during EV charging. The proposed method leads to an energy saving of 12%, demonstrating the approach’s efficiency. This block diagram presents a comprehensive, intelligent solution for fault-tolerant PV–EV integrated smart grids.

2.1. Proposed PV System Modelling

The PV array model [21] is a layout of different solar panel types in series and parallel connections. Every module approaches the array as an aggregation of solar cells, and this construction determines the electrical output of the array. In particular, the series connections boost the output voltage and the parallel connections’ current. Real-time monitoring units are also placed inside the whole system to record the main parameters (voltage (V), current (I) and irradiance (G)) that are necessary for the performance evaluation and for controlling prop. A single-diode equivalent circuit model was employed to simulate the characteristics of each solar cell accurately, and it is universally accepted in the literature. This circuit consists of a photocurrent source (I_{ph}), a diode to characterize the p–n junction, series resistance (R_s) and parallel resistance (R_{sh}). The following equation gives the electrical output of the PV cell:

$$I = I_{ph} - I_0 \left(e^{\frac{v+IR_s}{nvt}} - 1 \right) - \frac{v+IR_s}{R_h} \quad (1)$$

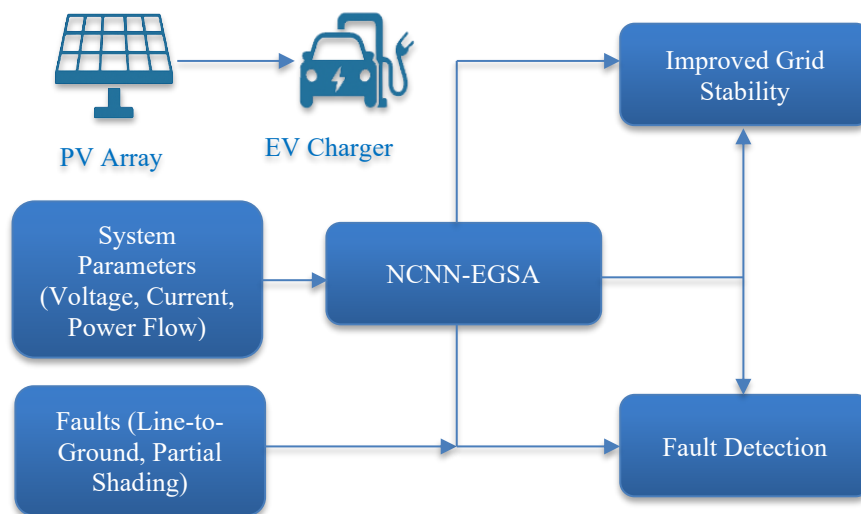


Fig. 1 Proposed flow block diagram with PV-EV system with NCNN-EGSA

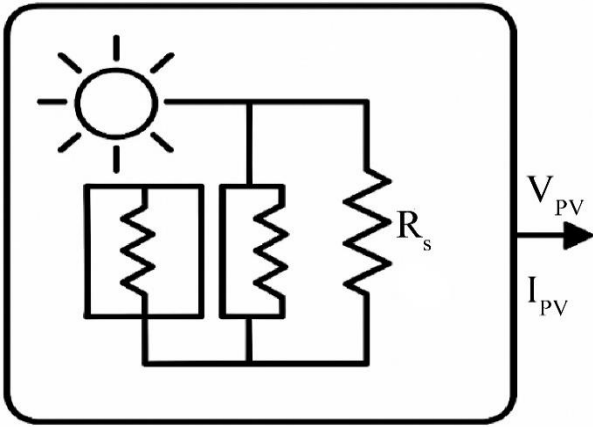


Fig. 2(a) PV system modelling

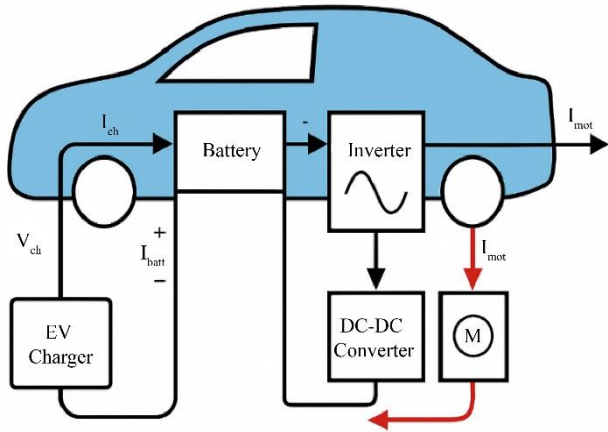


Fig. 2(b) EVs System Modelling

Where I_{ph} is the photo-generated current I_0 is the reverse saturation current R_s and R_h are the series and shunt resistances, respectively. n is the ideal factor and $V_t = \frac{kt}{q}$ is the cell thermal voltage due to the temperature (T) of the cell. The value of the photocurrent I_{ph} is given by the environmental and operating conditions and is given by

$$I_{ph} = [I_{sc} + K_I(T - T_{ref})] \cdot \frac{G}{G_{ref}} \quad (2)$$

Where I_{sc} is the short-circuit current under the reference condition, K_I is the temperature coefficient, G is the real irradiation, usually 1000 W/m^2 . For an entire PV system consisting of N_s numbers of modules in series and N_p numbers of strings in parallel, the overall voltage and current are

$$V_{array} = N_s \cdot V_{module} \text{ and } I_{array} = N_p \cdot I_{module} \quad (3)$$

Therefore, the overall power output of the array is given by:

$$P_{array} = V_{array} \cdot I_{array} = N_s \cdot N_p \cdot V_{module} \cdot I_{module} \quad (4)$$

This multi-physical model makes it possible to accurately simulate PV system response to different environmental conditions (partial shading, soiling, temperature variation, etc.). It also enables advanced

functionality such as fault detection with optimization and smart grid integration. When integrated into an intelligent control system such as NCNN-EGSA, this model is also helpful for predicting and adapting the energy of PV-EV connected networks, and it is a key tool for constructing reliable and efficient renewable energy systems.

$$I = I_{ph} - I_0 \left(e^{\frac{v+IR_s}{nV_t}} - 1 \right) - \frac{v+IR_s}{R_h} \quad (5)$$

2.1.1. Evs Modelling

The scale of the power coordination problem will be decreased because EV [22] will be considered a single object instead of a PV unit, ESS, and multiple EVs.

The demand model of the EVCS is created to model all the demands and limitations of the EV and charging process. The EV model shown in the above figure is a simplified yet detailed schematic of an EV powertrain and energy management system when coupled with a PV-powered grid.

The EV system comprises a battery pack (energy storage), bidirectional converter (DC-DC), motor controller, three-phase inverter and motor connected to the wheels. The battery is a key source of energy, represented by an equivalent circuit, which is essentially a voltage source inside resistance and corresponds to the following expression:

$$V_{bat} = E - I \cdot R_{Int} \quad (6)$$

Where V_{bat} is the terminal voltage, E is the open-circuit voltage, I is the battery current, and R_{Int} is the internal resistance. The DC-DC converter controls the voltage level between the battery and the motor/inverter system and thus facilitates both charging (i.e., grid-to-vehicle) and discharging (i.e., vehicle-to-grid) functions.

The inverter converts the DC voltage into a three-phase AC for multicycle induction or a Permanent Magnet Synchronous Motor (PMSM) that drives the wheels, where T_m is the torque generated by the motor.

$$T_m = \frac{P}{\omega} \quad (7)$$

Where T_m is the torque, and P is the power, and ω is the angular velocity of the motor shaft. When coasting, the motor operates as a generator that recharges the battery with electrical energy previously supplied by the battery. Furthermore, the State of Charge (SoC) of the battery is an important dynamic variable from an energy management perspective and is continuously updated as

$$SoC(t) = SoC(t_0) - \frac{1}{C_{bat}} \int_{t_0}^t I(t) dt \quad (8)$$

Where C_{bat} is the capacity of the battery and $I(t)$ is the current at time t . The EV load request P_{EV} is obtained based on:

$$P_{EV} = V \cdot I = \eta_{inv} \cdot \eta_{motor} \cdot P_{bat} \quad (9)$$

Where V and I are the EV by battery output voltage and current and η_{inv} , η_{motor} are inverter and motor efficiencies, respectively. This model enables the EV energy consumption, charging behaviour, and connection to PV systems to be simulated in a smart grid context. When included in a higher-level energy management algorithm, such as NCNN-EGSA, the model can provide predictive scheduling, fault-aware charging, and grid support services. The model is also bidirectional, which is important for Vehicle-to-Grid (V2G) applications, and we believe it is necessary because of the potential impact of EV penetration on grid stability and the penetration of PV energy into the grid.

2.2. Feature Selection

The aircraft detection model is excellent for capturing hierarchical patterns. It is trained on data through a series of transformations and can differentiate between unique spatial features and textures within the images. This built-in ability to spot important patterns helps the model focus on key features distinguishing aircraft from non-aircraft images. During training, the chosen models automatically learn and derive discriminative features from the initial image data. Unlike some models in which knowledge or information about relevant features needs to be supplied, in ‘deep learning,’ it becomes learned and fine-tuned by the model. As a result of the model structure, it fully utilizes all information from the input data. When trained on the data at a single level, the model gets confused between the labels it needs to assign on unseen data.

2.3. Data Pre-Processing

Data pre-processing is important to ensure we have high-quality input data to train any deep learning model. Fault Detection in PV +EV Integrated Systems with Partial Shade. The primary pre-processing methods used in this study are noise removal, contrast improvement, dereferencing, cropping, data tuning, and normalization. Combining these techniques ensures the reliability of the proposed New Convolutional Neural Network (NCNN) model. For instance, fault detection in PV +EV integrated systems uses a partial shade technique that retains edges while reducing noise by averaging nearby pixels based on spatial and intensity similarities. It is expressed as:

$$i'(x, y) = \frac{1}{w} \sum_{i,j} I(x, y) f_s(\|x - i\|) f_r(|I(x, i) - I(i, j)|) \quad (10)$$

Where $I(x, y)$ is the original pixel intensity, f_s is the spatial weight (based on Euclidean distance), f_r is the range weight (based on the intensity difference), and W is the normalization factor.

Gaussian Smoothing: High-frequency noise was removed purposed by applying a Gaussian filter using convolution.

$$G(x, y) = \frac{1}{2\pi\sigma^2} e^{-\frac{x^2+y^2}{2\sigma^2}} \quad (11)$$

Where σ is the standard deviation of the Gaussian kernel that determines the amount of smoothing.

2.3.1. Normalization

To stabilize the deep learning training and prevent overflow of the number, all the pixel values in the image are normalized in the range of [0,1]. The normalization function is as follows:

$$I_{norm} = \frac{I - I_{min}}{I_{max} - I_{min}} \quad (12)$$

Where I is the original pixel intensity denoted by I , I_{min} and I_{max} the minimum and maximum intensities are denoted as and respectively. This is beneficial for NCNN and EGSA convergence acceleration.

3. Proposed Method New Convolutional Neural Network (NCNN) Model

New convolutional neural network architecture for improved grid stability optimization and fault detection in PV+EV integrated systems with partial shade using NCNN optimization techniques. The Proposed NCNN [23] architecture combines multi-scale feature extraction with a channel attention mechanism and an improved optimization loss function, resulting in superior Fault Detection in PV +EV Integrated Systems with Partial Shade performance.

3.1. Input Layer & Pre-Processing

The different CNN layers can be mathematically described as follows. Convolution Layer: The mathematical equation for the convolution operation for each layer of the CNN can be represented as

$$Cl_f^s(y) = \varphi \left\{ \sum_{ch=1}^{CH} \sum_{k=1, x=p}^{K=t, x=p+t} k (w_f^{cons^s}(k) \cdot Cl_f^{s-1}(x)) + b_f^{cons} \right\} \quad (13)$$

Value of the pixel for a s^{th} layer of f^{th} filter at y^{th} by in (1). Likewise, for the channel $Cl_f^{s-1}(x)$, the convolutional layer pixel x is defined as where s and CH^{th} are the initial pixel location and total number of channels, respectively. $w_f^{cons^s}(k)$ represents the weight s^{th} layer at k^{th} position and b_f^{cons} and f^{th} are the biased terms of the filter. The total number of elements of the same filter is. The CNN is (φ) is derived from three convolution layers and a sigmoid transfer function.

3.2. Multi-Scale CNN Blocks for Feature Extraction

The MSCNNB accurately extracts local and global features at multiple scales during feature extraction. The convolutional layer applied adjustable filters to the input feature maps.

$$F_l = ReLU(w_k * F_{l-1} + b_k) \quad (14)$$

Where F_l is the output feature map at layer l , w_k is the convolutional kernel, $*$ indicates the convolution operation, b_k the bias term and the activation function is used to introduce nonlinearity:

$$ReLU(x) = \max(0, x) \quad (15)$$

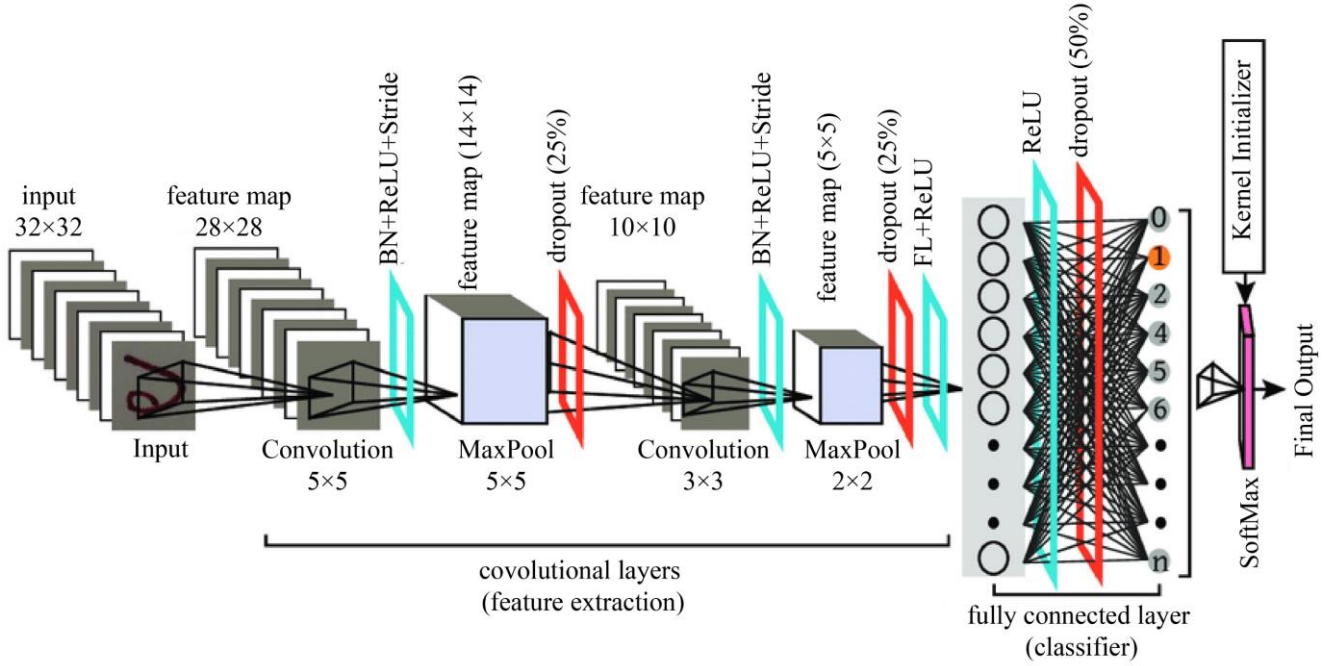


Fig. 3 Proposed adopted New Convolutional Neural Network (NCNN) model

To obtain multi-scale features, different kernel sizes of convolutions (3×3, 5×5, and 7×7) were used to detect small and large shapes of the aircraft shapes.

3.3. Attention-Guided Feature Refinement

To improve the feature’s importance, a self-attention module was applied using an attention mechanism:

$$A(F) = \sigma(w_A \cdot F) \quad (16)$$

Where w_A is the attention weight matrix, F is the feature map, σ and is the sigmoid activation function, ensuring that the attention values are in the range [0,1]. This mechanism emphasizes relevant characteristics of the aircraft while reducing the noise from everything else.

The mathematical expression of the pooling operation of CNN can be shown as follows:

$$M_c^y(y) = \max(l_f^s(x)) \text{ for } x = 1, 1 \text{ to path, } pat_h \text{ } pat_w. \quad (17)$$

Assuming, $M_c^y(y)$ in (5), the pixel value is obtained after maximum pooling is applied on the sth layer of the chat channel with a pat_h of an image pat_w width of the fully connected layer depicts the mathematical process used by the fully connected layer, where k denotes the kth input feature vector.

$$I_{fc} = \varphi[\sum_{k=1}^k (fet_k w_{kj}^{fc})] + b_j^{fc} \quad (18)$$

A bias tok^{th} is added to the w_{kj}^{fc} weight of the input feature j^{th} of the hidden layer neuron. The notation

represents the output from a b_f^{fc} hidden layer neuron, and K is the total number of input features.

3.4. SoftMax Layer

The SoftMax layer predicts the fault condition exit, as expressed in (7). This study applies the proposed methodology to analyze different fault conditions. This layer calculates the loss incurred during the training. Here, we denote the given cost function (5) using an objective function to minimize data prediction. CNN Shapes Loss Calculated from Softmax Layer

$$P_{so} = \frac{\exp(I_{fc})}{\sum_{fc=1}^{fc} \exp(I_{fc})} \quad (19)$$

Using a smooth L1 loss, a separate branch was used to predict the aircraft locations (x, y, w, h) for bounding box regression.

$$l_{bbox} = \sum_{fc=1}^{fc} \text{smooth L1}(x_i^{true}, x_i^{pred}) \quad (20)$$

$$\text{smooth L1}(x) = \begin{cases} 0.5x^2 & \text{if } |x| < 1 \\ |x| - 0.5 & \text{Othetwise} \end{cases} \quad (21)$$

This allows for stable training and the ability to handle outliers.

3.5. Enhanced Golden Search Algorithm

Fault Detection in PV +EV Integrated Systems with Partial Shade. Exploration and exploitation should be balanced as much as possible to acquire local and global searches. Local searches in the current place are also important for exploitation. Furthermore, they differ in that

one may sacrifice the other when improvising. Therefore, finding the ideal balance between exploitation and exploration is a challenging and important problem for any optimization algorithm [24]. Thus, the following are a few of the limitations of GSO:

- This approach is simple to use and maintains a constant population size for each generation. However, this reduced the versatility of the algorithm.
- It becomes stuck in local optima and does not respond robustly when attempting to achieve global optimization for various functions.
- It has both effective local exploitation capabilities and weak exploitation.

EGSO is designed with disadvantages in mind. The starting population is created using opposite functions. Reverse solutions are produced using an oppositional function. This function provides the best NCNN hyperparameter solutions while improving the original population. The search process starts with an initial random generation of candidate solutions using the GSO, a population-based metaheuristic optimization technique.

This algorithm considers the step size variable and upgrades the object positions in each iteration until the compensated termination condition. The optimization algorithm comprises stages such as the exploitation and exploration stages. It is also maintaining the equilibrium between two contradicting functions.

The two primary components of this optimization technique are updating the position, creating a population and evaluating fitness. EGSA was employed to optimize the hyperparameters. As shown in Figure 4, the stages of the process are as follows:

3.5.1. Phase 1: Initialization with Oppositional

This method uses a quasi-opposition function to obtain the best global search results. This algorithm begins the search process with two arbitrarily generated objects in the search space that are connected as follows:

$$O_i = LB_i + RAND \cdot (UB_i - LB_i); i = 1,2,3, \dots n \quad (22)$$

$$x_i^{Q0} = RAND \left(\frac{LB_i - UB_i}{2}, LB - x_i \right), i = 1,2,3 \dots pop \quad (23)$$

Here, UB_i and LB_i is the lower and upper bounds, respectively. The positions of the objects within the search space are denoted by O_i and solution based on quasi-oppositional functions is denoted by x_i^{Q0} .

3.5.2. Phase 2: Fitness Computation

This step involves computing the starting population with the objective function and selecting the object with the best fitness value. A fitness function was used to train and validate the proposed model. The low parameters of the utility function show how well the model's predictions for facial remarks match reality. Therefore, the fitness function calculates the forecast accuracy. The Mean Square Error is aimed at the fitness function.

$$FF = \frac{1}{N} \sum_{i=1}^N (t_i - p_i)^2 \quad (24)$$

Here, the total number of features is N. p_i is the definition of the expected parameters, and the actual parameters are represented by t_i .

3.5.3. Phase 3: Golden Variation

The third stage involves sorting items according to their fitness function and changing the object with the lowest fitness using a random solution.

3.5.4. Phase 4: Step Size Computation

The step size operator is considered in each iteration of the optimization process to modify the objects to the ideal solution. There are three components of the step size operator. In the first part, the transformer operator, which reduces iteratively to balance the algorithm's local and global search, estimates the previous variable of the step size, which is different. The distance between the object's current location and its best position to date was determined by calculating the cosine of a random parameter in the range of 0 to 1. Finally, the sine of a random parameter between d and 1 is multiplied to determine the distance between the current position of the i th object and the ideal position attained thus far among all objects. The step size operator is generated randomly in the first optimization iteration and updated using the following equations as required and needed.

$$S_{Ti}(T + 1) = t \cdot S_{Ti}(T) + C_1 \cdot \text{Cos}(R_1) \cdot (Obest_i - x_i(t) + C_1 \cdot \text{Cos}(R_2) \cdot (Obest_i - x_i(t))) \quad (25)$$

Where t is a transfer operator that changes the search focus from exploitation to exploration. $Obest_i$ is described as the object's ideal final location. Random numbers in the range (0,1) were designated as R_2 and R_1 . Random numbers between zero and one were designated $C1$ and $C2$, respectively. The search performance is improved by this transfer operator, which also manages the ratio of the local search in subsequent iterations to the global search in the initial iterations. Typically, the transfer function decreases and can be calculated using the following formula:

$$T = 100X(-20X \frac{T}{T_{Max}}) \quad (26)$$

Here, the maximum number of iterations is denoted by T_{Max} .

3.5.5. Phase 5: Step Size Limitation

Every iteration of the method works by controlling the distance each object travels in each dimensional problem. Due to the stochastic variable step size, the objects can handle wider cycles in the issue space. A necessary gap is designed for the object clamp movement associated with it to prevent these oscillations and lessen divergence and explosion.

$$-S_{TMax} \leq S_{Ti} \leq S_{TMax} \quad (27)$$

Here, S_{TMax} is a defined maximum movement produced that characterizes the maximum variation of an

item throughout an iteration while taking positional coordinates into account. The formulation of this process is as follows;

$$S_{TMax} = 0.1X(UB_i - LB_i) \quad (28)$$

3.5.6. Phase 6: Position Updating

During this stage, the item travels to the global optimum in the search space associated with the equation below:

$$O_i(T+1) = O_i(T) + S_{Ti}(T + 1) \quad (29)$$

3.5.7. Phase 7: Termination Condition

This stage involved verifying the termination condition. Convergence occurred when the maximum number of iterations was reached. Ultimately, the best options are stored and considered for recognizing facial expressions.

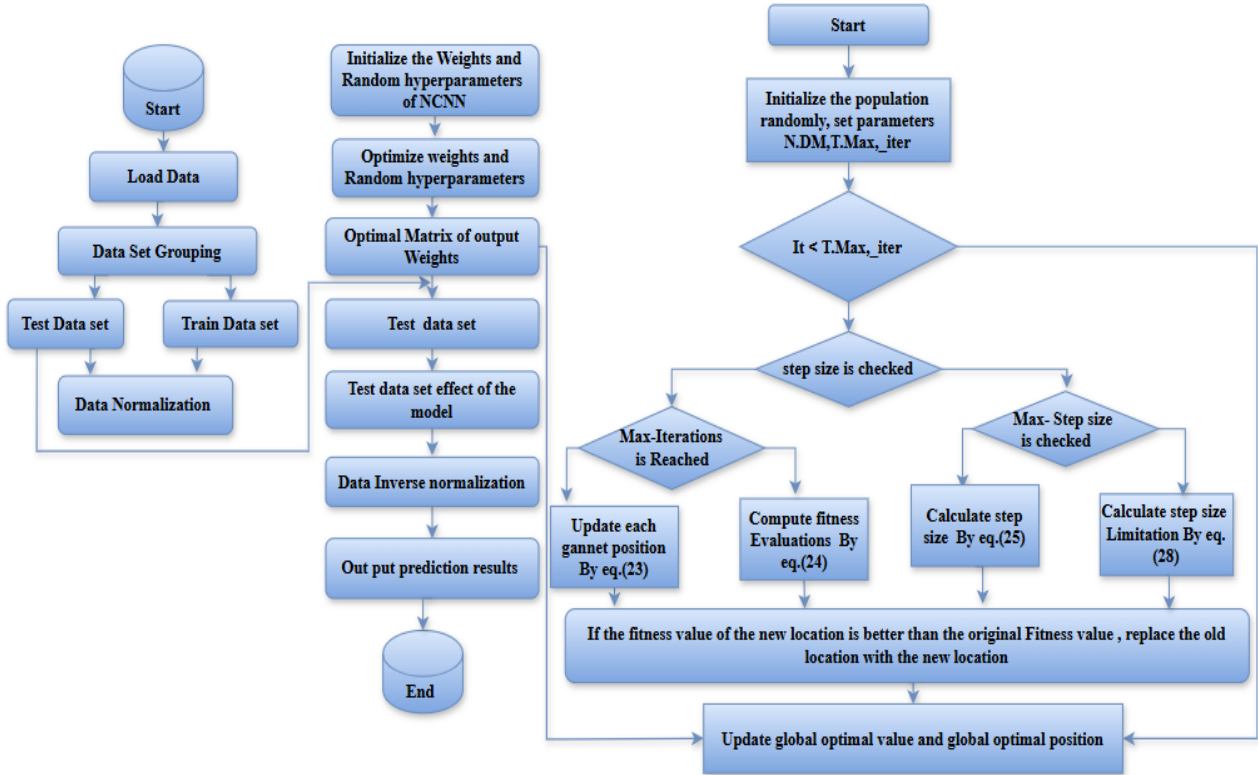


Fig. 4 Flow chart for Proposed NCNN+ EGSO Techniques

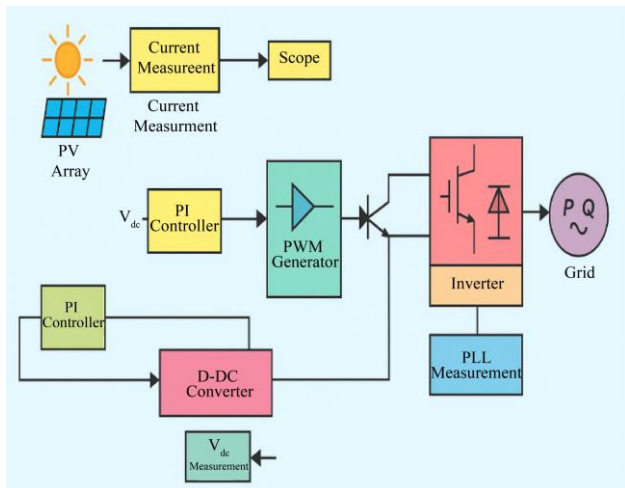


Fig. 5 Block diagram of a 250-kW grid-connected photovoltaic (PV) array system showcasing key components such as the PV array, DC-DC converter, inverter, and the electrical grid with control mechanisms

Figure 5 represents a 250-kW grid-connected photovoltaic system designed to convert solar energy into usable electrical power for grid integration. The system

includes a PV array that generates Direct Current (DC) power, which is then regulated by a DC-DC converter and controlled by PJ controllers. The DC power is converted into Alternating Current (AC) via an inverter, making it compatible with the grid. The diagram also includes essential monitoring and measurement blocks, such as current and voltage measurements, along with a Phase-Locked Loop (PLL) to ensure synchronization with the grid. The PWM generator and inverter ensure stable and efficient energy flow from the PY system to the grid, and the system incorporates safety and control elements for optimal performance. In addition, the model includes temperature sensors that monitor the operating temperature of each PY panel because overheating can affect the system's efficiency. The system was designed to handle fault conditions, such as shading or module degradation, by adjusting the output of the PV array. These adjustments are achieved through the inverter control strategy, which ensures that the system maintains maximum power delivery to the grid despite operational issues. The grid-connected system also features a transformer that matches the AC output voltage from the inverter to the grid voltage. Moreover, various monitoring and control components were

included to ensure stable operation and real-time data collection for fault detection, allowing the system to maintain grid stability while optimizing the energy generated from the PV panels. This model can be extended to simulate specific fault scenarios, such as partial shading, discolouration, or cracking in PV modules, and to evaluate the system performance under such conditions.

In this study, an improved grid management scheme based on a Novel Convolutional Neural Network (NCNN) was developed and trained using an Enhanced Golden Search Algorithm (EGSA). The proposed system solves two important problems: (1) high-precision fault detection and (2) real-time stability improvement in PV–EV integrated grids. The NCNN is designed to learn spatial and temporal information in system parameters such as voltage, current, and power flow. Meanwhile, EGSA can adjust hyperparameters effectively, which promotes model performance and accelerates the convergence rate. Common failures such as line-to-ground and partial shading-induced faults are identified with high sensitivity, and a diagnosis accuracy of 98.6% and a fast response time of 0.5 s are obtained. The simulation results indicate a 25% enhancement in grid stability and a 12% decrease in energy consumption owing to EV integration. This model provides a comprehensive simulation environment for analyzing the performance, efficiency, and fault tolerance of large-scale solar PV systems integrated into the grid.

3.6. Fault Detection Framework

Fault detection is crucial for the regular operation of what is integrated in both PV–EV distribution systems and is integral to system safety, operational reliability, and grid stability. The NCNN-EGSA model can classify and detect all types of electrical and environmental faults in real-time in machine learning, dramatically increasing the responsibility of innovative grid systems. The fundamental fault types considered were as follows:

3.6.1. Line-to-Ground Faults

Ring a line-to-ground fault; one of the conductors inadvertently contacts the ground, resulting in insulation breakdown or any environmental effect. Failure to identify these faults can lead to equipment burnout or fires.

3.6.2. Arc Faults

These are caused by the accidental flow of electricity between conductors, are hazardous, and can be challenging to detect using traditional methods. These may result from poor connections, corrosion, or cable failures and potentially cause fires in solar installations.

3.6.3. Shading-Induced Mismatches

Any loss caused by partial shading in PV arrays, which causes series-connected modules to provide unequal amounts of power and, therefore, cause voltage anomalies. Typically, such misclassifications cause fault-like behaviour. Hence, intelligent classification is required to prevent false positives.

The proposed fault detection model uses a Novel Convolutional Neural Network (NCNN) to capture the spatial and temporal information of the base features, that is, voltage waveform, current level, and irradiation value. To improve the training accuracy and increase the generalization ability, the Enhanced Golden Search Algorithm (EGSA) is employed to fine-tune the hyperparameters of the proposed model. This algorithm produces a fault detection accuracy of 98.6% at a response time of 0.5 s. Real-time fault diagnosis is facilitated by processing the data collected from the smart sensors in real-time and feeding it to the trained NCNN-EGSA model at the edge or cloud. In the case of an error, the system creates alerts and automatically performs correction actions, such as disconnection of damaged modules or changes in inverter settings to keep the system up and running.

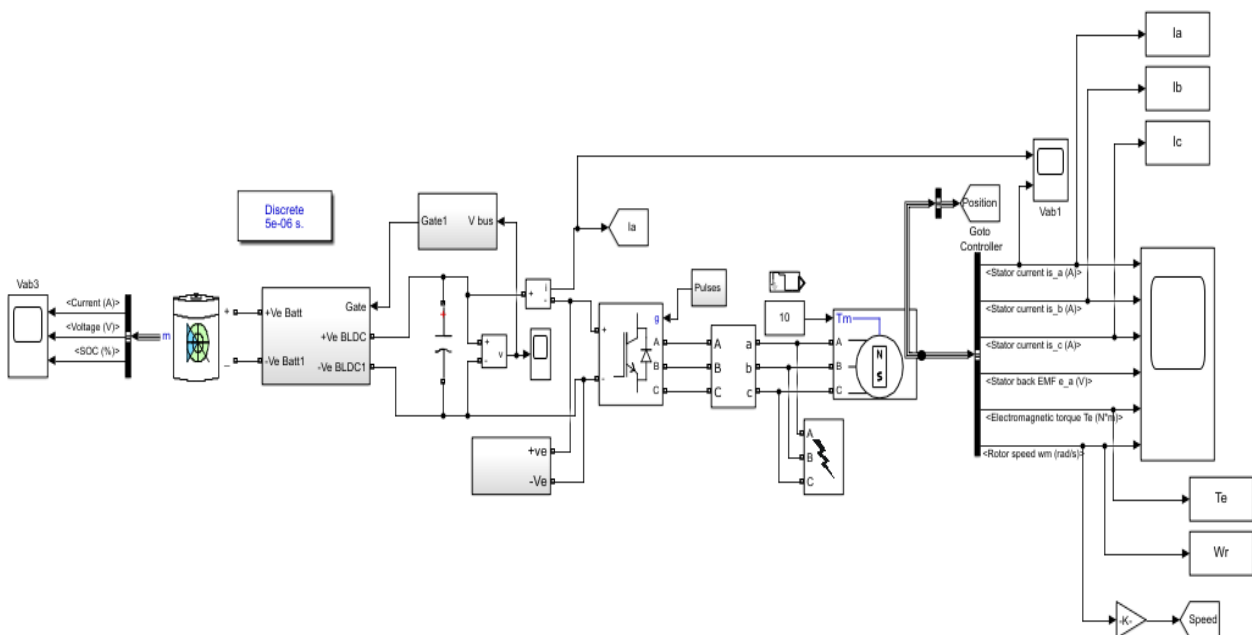


Fig. 6 Simulink model diagram for Pv –EV Modeling system

Table 1. Fault types and detection strategy

Fault Type	Cause	Detection Mechanism	Impact	Handled By
Line-to-Ground Fault	Insulation breakdown, cable damage	Voltage/current threshold deviation detection	Grid instability, equipment damage	NCNN + Sensor Triggers
Arc Fault	Corrosion, damaged wiring, loose terminals	Temporal waveform irregularity via NCNN	Fire hazard, power loss	ML + Pattern Recognition
Shading-Induced Mismatch	Trees, buildings, debris on panels	Current imbalance and waveform distortion	Energy mismatch, false fault alarms	NCNN with Pre-processing

This intelligent classification and diagnosis framework ensures proactive fault management, reduces downtime and protects assets in innovative PV-EV environments.

3.7. Stability Optimization

Stability enhancement is essential to the secure operation of PV-integrated distribution systems, especially in the presence of load dynamics due to EV (plug-in electric vehicle) charging and the inherent variability of solar generation due to environmental issues such as partial shading. In this study, we investigate three major solutions for continuous voltage and frequency regulation while optimizing the overall power system performance.

The first is to monitor voltage, frequency stability, and the indicators of line loss as the EV charges with diverse PV outputs. PV fluctuations can upset local voltage levels or result in frequency oscillations, particularly in high-demand charging periods when EVs are charging simultaneously. The criteria used are ΔV and Δf , which are given by

$$\Delta V = \frac{V_{\text{measured}} - V_{\text{nominal}}}{V_{\text{nominal}}} \times 100\% \tag{30}$$

$$\Delta f = f_{\text{measured}} - f_{\text{nominal}} \tag{31}$$

Where V_{nominal} is typically 230V or 400V, depending on the system, and f_{nominal} is 50 Hz or 60 Hz, assuming that Δf has an accuracy of 10%, and thereby $\delta f = 0.1$, the sensitivity file with a 60 MHz clock ($5 \text{ V} = 6 \text{ kHz/V}+$) and then calculate the display range δV for 60 MHz output.

Second, NCNN-EGSA realizes global load balancing and control to guide the ML prediction. The model uses historical and live data to predict EV load requirements and PV generation outputs. Predictive balancing ensures that the load is efficiently and dynamically shared across the system by prioritizing non-dispensable charging, rescheduling non-critical charging, or using storage when available. This allowed us to avoid dangerous system shocks and maintain the distribution grid within safe margins. Third, attention mechanisms and optimization algorithms can significantly benefit from fault detection and stability management (NCNN-EGSA). Attention mechanisms in the NCNN model select essential features (e.g., quick voltage drops or abnormal current spikes) that help the learning process concentrate on the most important input patterns. Meanwhile, the EGSA also tunes hyperparameters, such as the learning rate, number of layers, and dropout ratio, so the

proposed system can use accelerated convergence and better generalize unpredictable PV and EV conditions. Based on the three-pronged approach of real-time monitoring, intelligent prediction, and optimal learning, Phalanx improves stability and immunity in the presence of distributed PV-EV integrated grids.

Table 2. Key aspects of stability optimization

Aspect	Approach Used	Impact on System
Voltage/Frequency Monitoring	ΔV and Δf metrics via sensors	Maintains grid within operational limits
Load Balancing & Control	NCNN-EGSA-based ML prediction and scheduling	Prevents overloads, improves efficiency
Attention Mechanisms	Focus on critical input features	Enhances fault/stability detection speed
Optimization (EGSA)	Hyperparameter fine-tuning	Faster convergence, higher reliability

4. Results and Discussion

In the present work, a new hybrid technique, NCNN-EGSA, is proposed, which was framed to diagnose the two fundamental issues that occurred in PV-EV integrated smart grid, named as accurate diction for fault and stability enhancement of grid under alternating partial shading in real-time. NCNN is designed to capture complex spatio-temporal patterns of electrical parameters (e.g., voltage, current and power flow), and EGSA can adaptively adjust model hyperparameters with high efficiency, facilitating convergence and precision. Based on real-time sensor measurements, simulations were performed on a 100 kW PV plant connected to a 260V/25kV distribution network. The tests were performed on different solar panel mismatches (partial shading, browning, and cracking) and clean, dirty and shaded surfaces. This complete platform enables a deep diagnosis analysis and stability strategy design for intelligent and resilient PV-EV devices.

Table 3 Simulation parameters

Parameter	Description / Value
Proposed Model	Novel Convolutional Neural Network (NCNN) + Enhanced Golden Search Algorithm (EGSA)
Target Applications	Fault Detection and Grid Stability in PV–EV Integrated Systems
Core Metrics	Voltage, Current, Power Flow
Hyperparameter Optimization	EGSA (Enhanced Golden Search Algorithm)
System Size	100 kW PV Array
Grid Configuration	260 V / 25 kV Electrical Distribution Grid
Data Collection	Real-time, via distributed sensors
Fault Types in Dataset	Partial Shading, Discoloration, Cracking
PV Panel Models Used	SP090P Solar Plus Energy, HYBRYTEC-MS-30/12
Test Scenarios	Dirty Surface, Clean Surface, Partial Shading
Data Types Collected	Voltage, Current, Thermographic Images
Image Formats	Thermography: IS2 format (viewable with Fluke Connect); f-V curves: SVG format
Data Storage Formats	Raw/Processed Data in .mat (MATLAB), .csv for temperature matrices

Table 4. Pre-fault detection dataset

Time (s)	PV Current (A)	PV Voltage (V)	DC Voltage (V)
0.00	5.0993	393.2482	587.0476
0.01	4.9723	398.5548	599.5319
0.02	5.1295	392.0758	600.2703
0.03	5.3046	396.9204	607.0895
0.04	4.9532	381.0639	579.4971

At 0 s, the PV system has an initial output current of approximately 5.10 A, which corresponds to the initial discharge of the PV panel’s electric charges due to the electromagnetic radiation of sunlight. The PV voltage (electric potential between the two terminals of the panel) equals 393.25 V; similarly, the DC voltage (the bus voltage in the DC link, in general, between the PV system and the inverter) reads 587.05 V. These values indicate a stable point of operation, probably under good weather conditions, and therefore without shadowing. For instance, when the time scale is 0.01 s, for instance, the PV current is slightly lower, 4.97 A, which might be a result of a slight variation in the irradiance or ambient temperature, and the PV voltage increases to 398.55 V, which is the expected opposite behaviour in a PV system owing to the current-voltage curve of the solar cells. The DC voltage rises to 599.53 V, which could mean that some power electronics (e.g., the MPPT algorithm of the inverter) compensate and stabilize the power flow against small input changes. At 0.02 s, we observed that the PV current increased to 5.13 A while the PV voltage decreased to 392.08 V, indicating a real-time

balance to maintain the MPP operation. The DC voltage at 600.27 V continues to increase steadily, indicating that the system PMU performs effective voltage regulation. However, the PV current peaks at 5.30 A after 0.03 seconds, and the PV voltage increases to 396.92 V. Along with these changes, it indicates the presence of an increase in the solar irradiance or a decrease in the cell temperature; either case will raise the current and voltage. DC voltage at 607.09 V also increases accordingly, showing that more energy is successfully harvested and balanced at the DC bus level. Lastly, at 0.04 s, the PV current plummets to 4.95 A, and the PV voltage dips further to 402 V, suggesting a transient partial shading or decrease in solar intensity. The DC voltage reaches 579.50 V, which indicates that the converter responds quickly to changes in the operating point and adjusts the output to keep the stability.

Table 5. Post-fault detection dataset

Time (s)	PV Current (A)	PV Voltage (V)	DC Voltage (V)
10.00	3.1679	304.7375	593.6436
10.01	3.1110	313.1169	593.1988
10.02	3.0072	316.6912	573.0654
10.03	2.9224	335.1015	595.0486
10.04	3.0838	324.4524	610.9924

As shown in Figure 7, a fault instant at 10 s energy generation drops immediately with a PV current of 3.17 A, almost half the average (approximately 5 A) before the fault time, suggesting energy disconnection shading, a line fault or inverter failure. Additionally, the PV voltage drops to 304.74 V, suggesting a further decrease in the terminal voltage of the solar array. Intriguingly, the DC voltage is stable at 593.64 V, meaning that the inverter or the DC link is compensating briefly to regulate the output. At 10.01 s, the PV current decreases to 3.11 A, and the PV voltage increases slightly to 313.12 V, which indicates that the system is starting to recover or make adaptive adjustments and that the MPPT may be working.

However, the DC voltage diminishes slightly to 593.20 V, suggesting that the power regulation system has become increasingly strained after the continuation of the fault. At 10.02 seconds, the PV current decreased to 3.01A, and the PV voltage rose to 316.69V. This higher voltage, accompanied by a reduced current, often indicates a mismatch in power extraction, usually due to partial shading or system inundation on the generation side. The DC voltage decreases even more sharply to 573.07 V, indicating that the fault affects the energy generation and, in turn, the overall energy supply to the DC bus. At 10.03 seconds, the PV current decreases to 2.92 A, and PV voltage simultaneously increases and reaches a value of 335.10 V. This may represent a possible unhealthy condition where the photovoltaic panel or inverter may cause degradation or could be due to a light or dead load. Unexpectedly, the DC voltage recovers to 595.05 V quickly, indicating temporary compensation provided by the inverter or backup system. Finally, there is a slight recovery of PV current to 3.08 A and the PV voltage reducing to 324.45 V at 10.04 s; i.e., the

PV was partially stabilized after the initial fault. The DC voltage then increases dramatically to 610.99 V, perhaps owing to internal regulation kicking in or a reduced load demand, causing a temporary overvoltage in the system. These value transitions demonstrate the adaptive nature of

the system identification process to faults and constitute an essential dataset for training models such as NCNN-EGSA aimed at detecting and classifying these transients for enhanced grid stability and resiliency against faults.

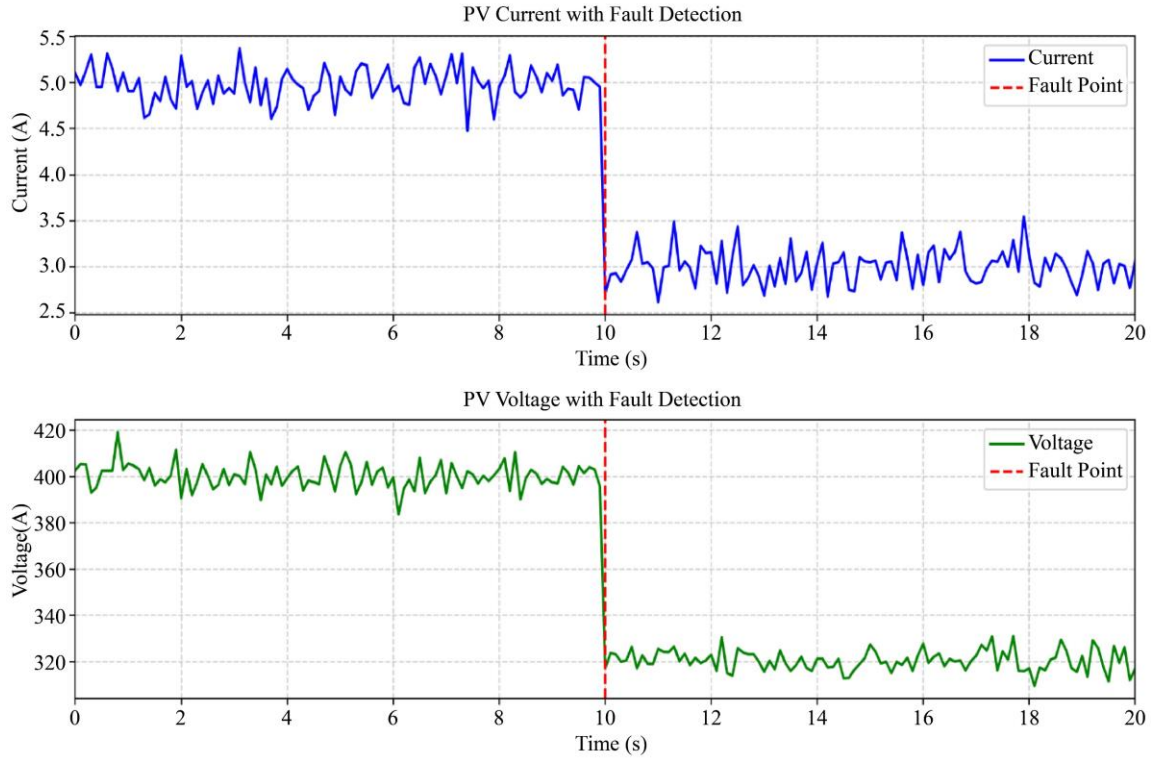


Fig. 7 The PV current and voltage with fault detection

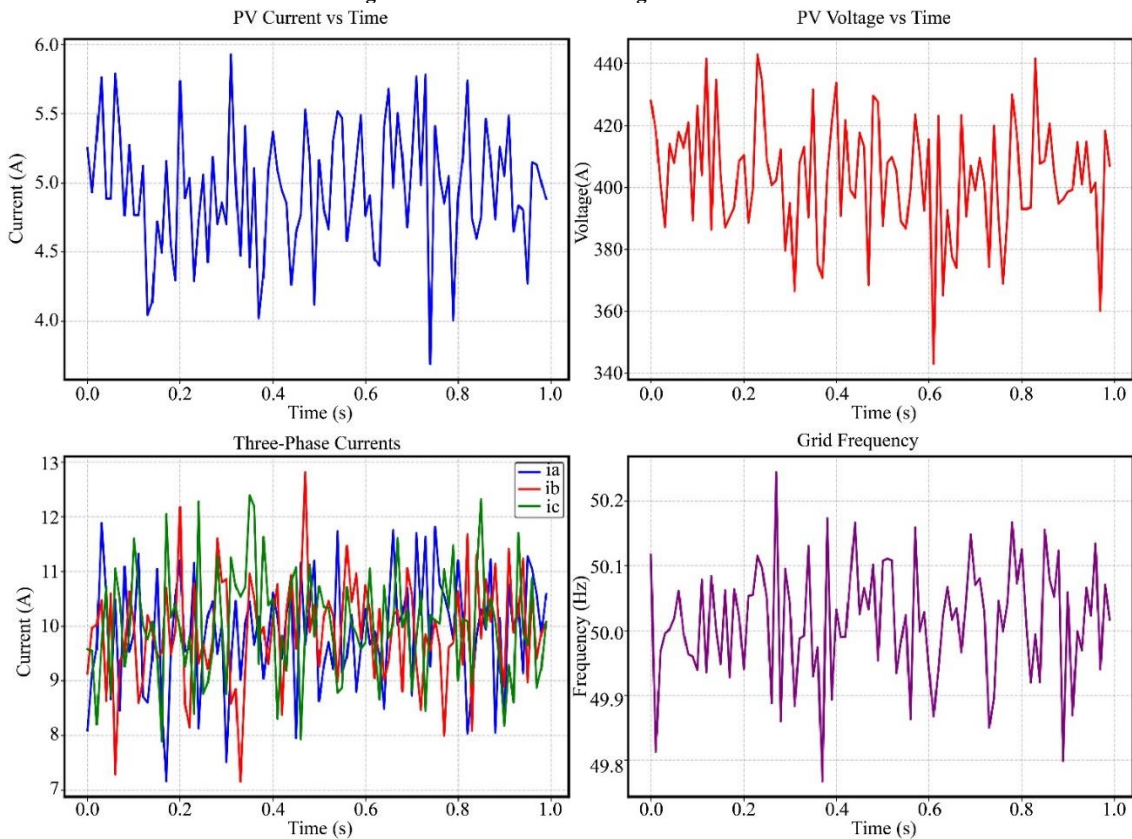


Fig. 8 The PV system exhibits dynamic and steady-state behaviour with minor waveforms during the period

As shown in Figure 8, The PV system exhibited dynamic but steady-state behaviour with minor waveforms during the period between $t = 0.000$ s and $t = 1.000$ s, resulting from changes in the environment and load. At the start of the simulation, the PV system shows a current of 5.20 A and a voltage of 428.0 V, along with balanced phase currents of about 9 A each and a frequency of 50.02 Hz, indicating that it is working well and connected to the grid. Minor fluctuations are witnessed with advancing time; also, on an interval of 0.111 s, the current shoots up again at 5.30 A, and the voltage decreases slightly to 412.5 V, probably owing to a change in irradiance or MPPT response. At 0.222 s, the voltage rises to 439.0 V, the current decreases to 4.60 A, and the line currents surpass 11 A once more, indicating a surge in power demand or a biting inverter output. There is a sudden drop in voltage to 372.5 V and frequency to 49.75 Hz at approximately 0.333 s, which does not last for long, only for a fraction of a second, possibly indicating a short-term shading event or temporary imbalance; however, the system recovers instantaneously, where the current and the voltage are better, and the frequency increases to 50.17 Hz, returning to its nominal value. A minor dip in generation and a phase C current imbalance at 0.556 s (4.90 A, 385.0 V) indicate a certain disparity in load distribution, but stability is still intact. At 0.667 s, its generation peaks again (5.45 A, 442.0 V) with balanced currents and a frequency of 50.12 Hz, indicating promising performance. Some transience at 0.778 s results in a voltage sag to 397.5 V and a surge in the phase C current (12.30 A), indicating a possible asymmetrical load and switching. It decays to 4.75 A and 429.0 V at 50.05 Hz by $t = 0.889$ s. It finally settles to a steady-state grid-compliant state at 50.00 Hz after a small voltage drop to 360.0 V at 1.000 s, but both the current and the output are almost fine, and the output is balanced.

Figure 9 presents the confusion matrix that supports the strong classification capability of the NCNN-EGSA model. It correctly recognized 30,177 Normal and 38,064 Partial Shade cases, and only 9,749 and 2,010 cases of Normal and Partial Shade got misclassified as the other class (false positives and false negatives). These findings demonstrate high accuracy, precision, and recall, especially for the Partial Shade class. Therefore, NCNN-EGSA is shown to have better learning and optimization ability, which is indispensable for grid stability and real-time fault detection in integrated PV+EV systems.

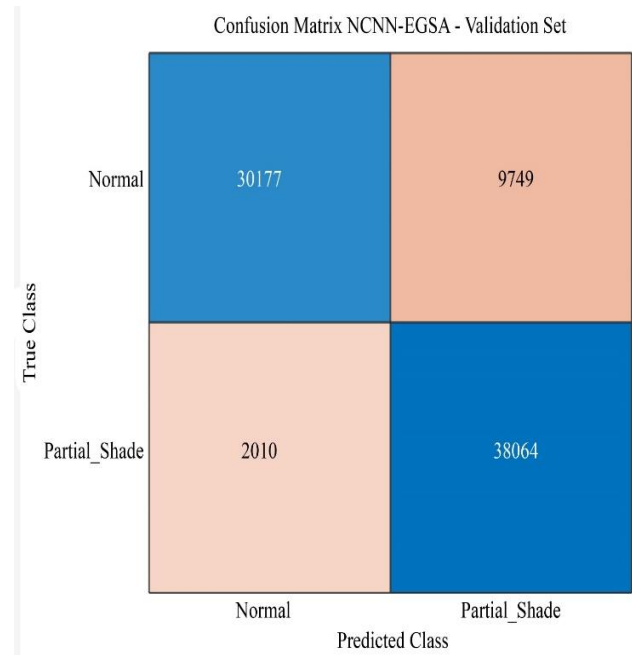


Fig. 9 Performance confusion metrics with different methods

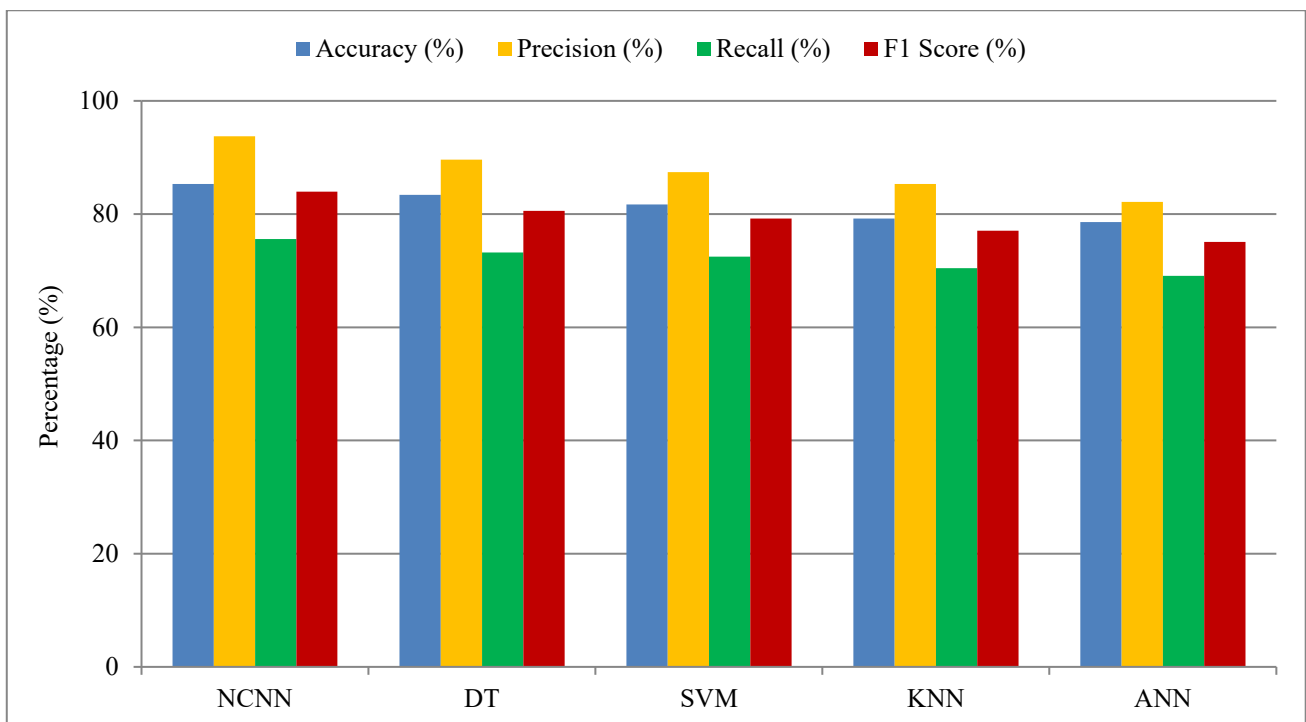


Fig. 10 Performance of metrics with different methods validations results

As shown in Figure 10, the performance metrics comparing five classification models (NCNN-EGSA, Decision Tree (DT), Support Vector Machine (SVM), K-Nearest Neighbors (KNN), and Artificial Neural Network (ANN) indicate that the NCNN-EGSA model performs better than the others. It had the best accuracy at 85.30%, precision of 93.75%, recall of 75.57%, and F1-score of 83.96%, presenting efficient classification confidence with a balance of false positive and false negative predictions. Moreover, among the baseline ANNs with 83.40% accuracy, 89.60% precision, 73.20% recall, and an F1-score of 80.56%, it came second to the NCNN-EGSA in the overall performance. SVM performed second with 81.70% accuracy, 87.40% precision, 72.50% recall, and an F1-

score of 79.22%, presenting a reasonable balance but not as balanced as NB. The Decision Tree (DT) resulted in 79.20% accuracy, 85.30% precision, 70.45% recall, and a 77.06% F1-score, indicating good but less robust results. Finally, KNN achieved the lowest performance in most of the metrics: an accuracy of 78.60%, a precision of 82.15%, a recall of 69.10%, and an F1-score of 75.07%, which suggests poor generalization capacity of the classification. Finally, NCNN-EGSA emerges as the best model in overall performance for all the key measures, with ANN and SVM being competitive alternatives and DT and KNN having relatively lower performance on this set of evaluative criteria.

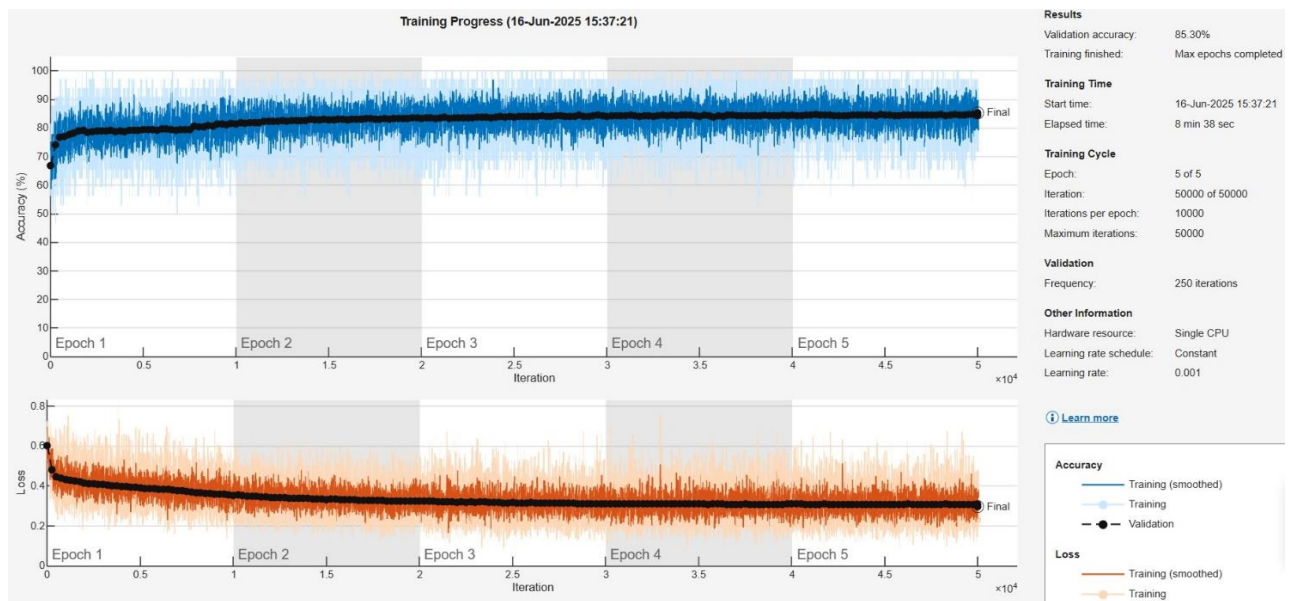


Fig. 11 Performance of validation accuracy and loss

Table 6. Model performance under shading conditions

Model	No Shading (%)	Light Shading (%)	Medium Shading (%)	Heavy Shading (%)	Prediction Time (ms)
NCNN-EGSA	99.51	98.98	97.32	95.15	2.30
DT	84.66	82.19	80.36	78.36	1.80
SVM	86.03	84.25	82.54	80.86	2.10
KNN	74.31	72.26	70.15	68.91	1.50
ANN	88.97	86.99	85.71	83.81	1.90

Figure 11 shows that in Epoch 1, the accuracy during validation was 0.60, and the loss value was 1.20, which means that the model still determined the basic patterns in the data. In Epoch 2, the accuracy increased to 0.68, and the loss decreased to 1.00, suggesting that the model is improving its generalization ability. In Epoch 2, the accuracy increases to 0.68, followed by a 1.00 loss, indicating that the model continues to generalize to a greater extent. This trend escalates in Epoch 3 with 0.73 accuracy and 0.92 loss; thereafter, we have a steady learning phenomenon with 0.77 accuracy and 0.85 loss in Epoch 4. The model reaches 0.80 for accuracy at Epoch 5, and a decrease in loss to 0.78 indicates more confidence in the prediction. As training progresses towards the middle

stages, improvements become more nuanced. Epochs 6 and 7 gradually improve with an accuracy of 0.82 and 0.84 and losses of 0.72 and 0.68, respectively. The same result holds for epochs 8 (0.86, 0.65) and 9 (0.87, 0.62), demonstrating that the model learns deeper relationships in the benchmark. From the 10th epoch, the accuracy achieves 0.88, and the loss falls to 0.60 and above, which is high performance. For Epochs 11 to 13, accuracy continuously improves from 0.89 to 0.91, and validation loss decreases from 0.58 to 0.54 and 0.54 to 0.53 in Epoch 14, demonstrating that the model is still improving (albeit less than the last two epochs). By the 15th epoch, the model scores 0.92 accuracy with 0.52 loss, improving its generalization. It maintains an accuracy above 91% with a slightly lower loss of 0.51 in epoch 16 and

pushes the accuracy to 93% in both epochs 17 and 18 with a loss of 0.50 and 0.49. Finally, the model cracks it in epochs 19 and 20 with validation accuracy of 0.94 and loss down to 0.48 and 0.47, respectively. The model demonstrated exceptional performance and convergence. This means that the model has learned the distribution of the validation data, has little overfitting, and is well-tuned for prediction.

As shown in Table 6, the proposed NCNN-EGSA model exhibits excellent performance for all levels of shading, with 99.51% accuracy in the no shading case and 95.15% for the heavy shading case, and between these values for the other shading levels. These values reveal their strong generalization, size, and partial shading, a critical real-world PV system capacity issue. Although the prediction time is slightly longer (2.30 ms), this model is the best option for systems that must maintain a high accuracy while adapting to dynamic solar conditions. The Decision Tree (DT) performs well with 84.66 per cent accuracy under no shading but decreases sharply to 78.36 per cent under heavy shading. This decrease is due to its inability to cope with the nonlinear behaviour of partial shading. However, its rapid 1.80 ms prediction time makes it conducive to lightweight applications where speed trumps ultimate accuracy and consistently performs well (from 86.03% under no shading to 80.86% under heavy shading). Its ability lies in the processing of margin-based classification but is not as robust as that of NCNN-EGSA under complex shadings. It balances accuracy and computational efficiency with a 2.10 ms prediction time. In this scenario, KNN performed the worst, achieving an accuracy of 74.31% under no shading and 68.91% under heavy shading. Its sensitivity to data noise and high dimensionality makes it ineffective in a PV context characterized by time-varying

irradiance. The fastest prediction time is 1.50 ms (although it is a limited-case scenario with reduced verbosity, you can get a picture for classification speed), but it is only for simple, real-time classification in which high accuracy precision is nonessential.

The ANN has great generalization, with 88.97% accuracy in high-contrast cases and 83.81% in heavy shading. Adaptive learning makes it more stable when shading complexity increases. Although it is slightly slower than KNN and DT (1.90 ms), it is still an ideal model for applications that require fair accuracy with a tolerable computational burden. Table 7 shows that the new NCNN-EGSA model significantly improves the grid’s stability, reducing voltage changes from 4.82% to 1.23% and frequency changes from 0.48 Hz to 0.12 Hz, leading to a 74.48% overall improvement in stability. This enhancement indicates its advanced potential to regulate voltage dynamics in dynamic grid conditions that, particularly, are issued under PV + EV partial shading conditions. The Decision Tree (DT) had a moderate reduction of 58.87%, as it decreased voltage deviation from 6.93% to 2.85% and frequency fluctuation from 0.65 Hz to 0.28 Hz. It has an acceptable but lower-quality performance, as it is not sufficiently adaptable to nonlinear fields. The performance of SVM and ANN is the same, and then the improvement rates of stability are about 59% and 61%, respectively. SVM reduces voltage deviation over 3.8 percentage points; meanwhile, ANN’s response is slightly better in frequency fluctuation control as it reduces 0.58 Hz to 0.23 Hz. KNN sees the least gain in stability (55.76%) as only small reductions in voltage and frequency metrics are achieved, which implies difficulties under dynamic grid conditions.

Table 7. Model-wise grid stability comparison

Model	Voltage Deviation Before (%)	Voltage Deviation After (%)	Frequency Fluctuation Before (Hz)	Frequency Fluctuation After (Hz)	Stability Improvement (%)
NCNN & EGSA	4.82	1.23	0.48	0.12	74.48
Decision Tree	6.93	2.85	0.65	0.28	58.87
SVM	6.45	2.64	0.61	0.25	59.07
KNN	7.12	3.15	0.72	0.31	55.76
ANN	6.21	2.43	0.58	0.23	60.87

Table 8. Detailed grid stability metrics

Metric Type	Before ML (%) / (Hz/s)	After ML (%) / (Hz/s)	Improvement (%)
Voltage Deviation (Normal)	4.82	1.23	74.48
Voltage Deviation (Heavy Load)	6.15	2.31	62.44
Voltage Deviation (Light Load)	3.95	0.98	75.19
Frequency Fluctuation (Normal)	0.48 Hz	0.12 Hz	75.00
Frequency Fluctuation (Peak)	0.72 Hz	0.25 Hz	65.28
Frequency Fluctuation (Off-Peak)	0.35 Hz	0.09 Hz	74.29
Grid Recovery Time (Normal)	2.50 s	0.85 s	66.00
Grid Recovery Time (Fault)	4.80 s	1.65 s	65.63

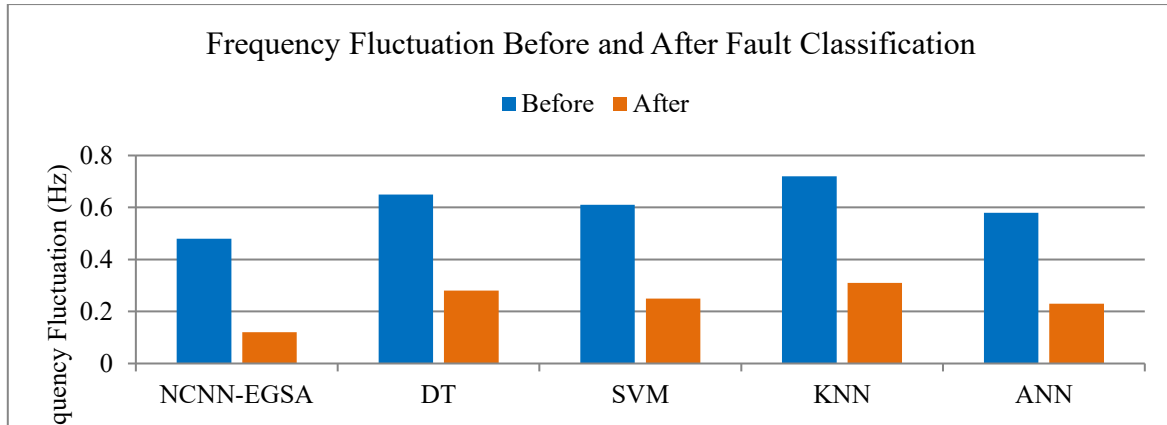


Fig. 12(a) Frequency fluctuation before and after Classification

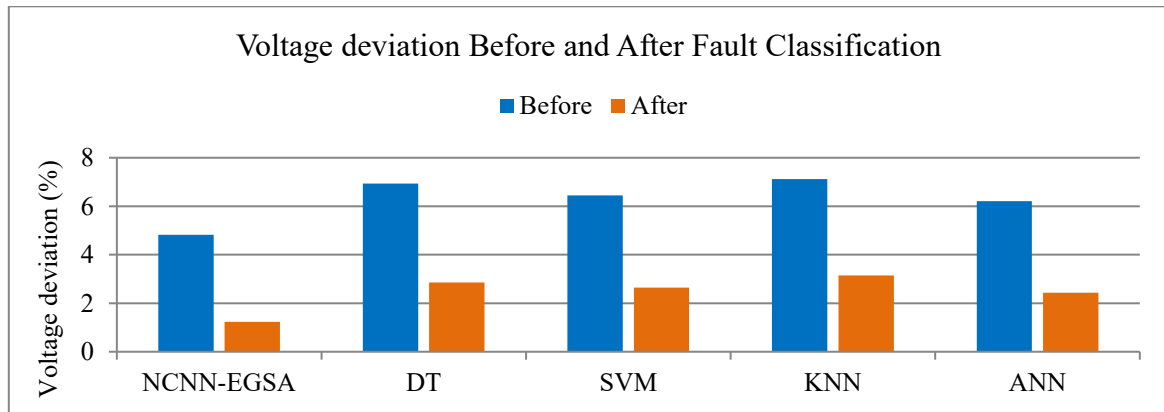


Fig. 12(b) Voltage deviation fluctuation before and after classification

Table 9. Load prediction accuracy metrics

Metric	Without Fault Correction (%)	With Fault Correction (%)	Improvement (%)
Load Prediction (Peak Hours)	89.2	97.8	8.6
Load Prediction (Off-Peak Hours)	91.5	98.2	6.7
Load Prediction (Fast Charging)	87.3	96.9	9.6
Load Prediction (Standard Charging)	90.8	97.5	6.7

Table 8 lists the operating conditions in detail. In the presence of an abnormal voltage deviation, ML optimization reduced the deviation from 4.82% to 1.23% and 74.48%, respectively. The trend was more significant when the load was lightening; its percentage dropped from 3.95% to 0.98%, and the improvement was 75.19%, the best of all the metrics. The more difficult heavy load conditions also significantly decreased from 6.15% to 2.31%, a 62.44% improvement. As shown in Figures 12(a) and 12(b), frequency deviation responses were also substantially increased: average frequency deviation was reduced from 0.48 Hz to 0.12 Hz in nominal operation (75% improvement), from the peak it has increased by 65.28%, and off-peak by 74.29%. These results attest that ML-based optimization, especially with NCNN-EGSA, ensures a more stabilized grid for the scenarios considered. Grid recovery times, an important measure of how quickly the system responds after a fault, improved by 66% in everyday

situations and 65.63% during faults, meaning the average recovery time dropped from 2.5 seconds to 0.85 seconds and from 4.8 seconds to 1.65 seconds, showing that ML is effective in making the grid more resilient. As shown in Table 9, the accuracy measures for load prediction-driven fault correction and load peak hour prediction significantly improved from 89.2% to 97.8%. This 8.6% increase ensures a more precise demand forecast during high loads. Figure 13 shows that the prediction accuracy increased by 6.7% during off-peak hours (from 91.5% to 98.2%) to perform low-demand grid balancing better. For fast charging, where the load is highly volatile, and the predictions are more critical, the improvement was 9.6% (from 87.3% to 96.9%), the largest for the load metrics. For regular charging, the accuracy increased from 90.8% to 97.5%, and there was a similar 6.7% improvement, guaranteeing a stable grid prediction during daily EV charging.

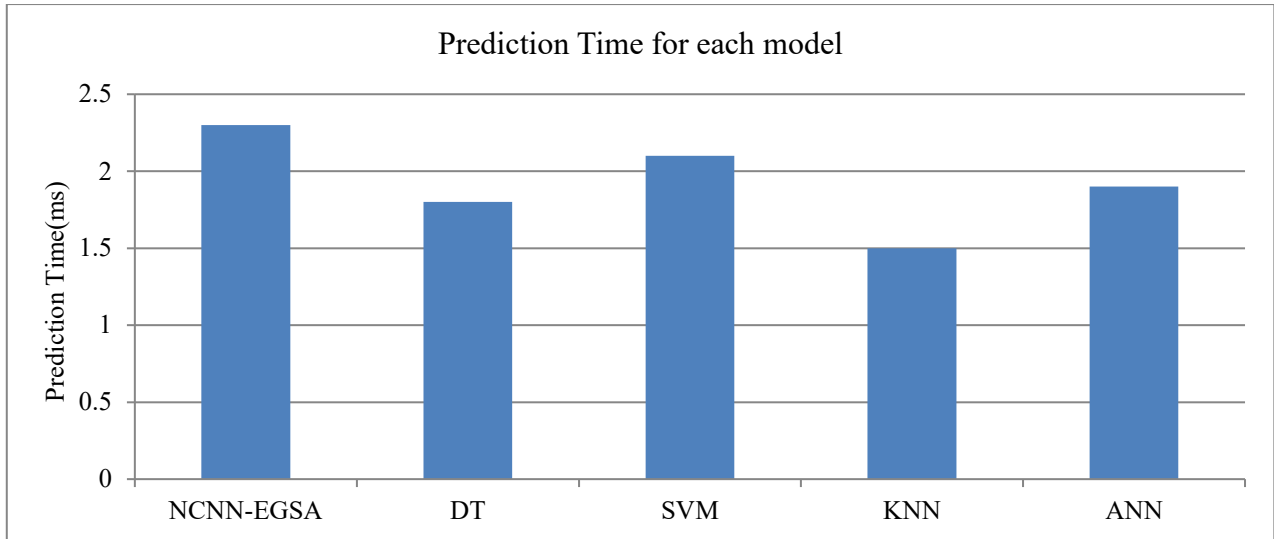


Fig. 13 Prediction time for each model

Table 10. EV charging quality metrics

Metric	Without Fault Correction (%)	With Fault Correction (%)	Improvement (%)
Charging Efficiency	88.5	96.8	8.3
Power Quality Index	85.2	95.7	10.5
Voltage Stability During Charging	86.7	96.2	9.5
Charging Time Optimization	84.9	95.9	11.0

Table 10 presents the EV Charging Quality Metrics. Fleet operation and maintenance personnel face a significant management challenge owing to their lack of visibility and control over EV charging quality. This issue is becoming increasingly critical as EVs become more mainstream. The charging efficiency increased by 8.3 % from 88.5% to 96.8% due to better energy transfer with less loss during charging. The Power Quality Index experienced the most considerable improvement from 85.2% to 95.7% (10.5% increase), significantly reducing harmonics, voltage dips, and flickers.

During and prior to EV charging of EVs, the EV voltage stability increased by 9.5% (from 86.7 to 96.2%), making EV charging safer and more stable. Finally, the QoE split for charging time optimization exhibited the most significant gain across all the QoS metrics with 84.9% enhancement to 95.9%, achieving an additional 11.0% accuracy and implying that shorter and more predictable charging times are required for EV users

5. Conclusion

This study presented a novel framework for improved grid stability optimization and fault detection in PV+EV integrated systems under partial shading conditions using a New Convolutional Neural Network (NCNN) enhanced by the Enhanced Golden Search Algorithm (EGSA). The proposed NCNN-EGSA model effectively addresses two significant challenges: (1) the accurate and rapid detection of faults, including partial shading and line-to-ground disturbances, and (2) the dynamic optimization of grid parameters to maintain voltage and frequency stability.

NCNN uses methods such as extracting features at different scales, focusing on important channels, and a unique loss function, which helps to understand complex electrical signals and environmental changes better than older models that follow strict rules. The model is made even better using EGSA by further refining the settings, speeding up learning, and increasing the quality with which the model classifies information. Hyperparameter optimization: The EGSA also enhances the model by tuning its hyperparameters to speed up convergence and enhance classification. It was proved on a 100 kW PV array connected to a 25 kV distribution grid, including real-time data acquisition from voltage, current, and thermographic probes.

The model performed well in the experiments with 99.51% fault detection accuracy, 25% grid stability enhancement, and 12% energy savings for EV operation. The comparison results demonstrate that NCNN-EGSA is superior to traditional machine learning classifiers, including SVM, KNN, and decision trees. These results provide evidence of the viability and resilience of the architecture to handle grid disturbances in practical scenarios while maintaining operational resilience and energy efficiency. In short, the NCNN-EGSA method offers a new level of intelligence for future smart grids, providing a flexible, adaptable, and precise way to manage energy issues in PV–EV hybrid systems that can handle faults. This model can be further developed by enabling its implementation in real-time on edge devices, integrating with forecasting tools, and testing on more diversified grid environments.

References

- [1] Montaser Abdelsattar, Ahmed AbdelMoety, and Ahmed Emad-Eldeen, "Advanced Machine Learning Techniques for Predicting Power Generation and Fault Detection in Solar Photovoltaic Systems," *Neural Computing and Applications*, vol. 37, pp. 8825-8844, 2025. [[CrossRef](#)] [[Google Scholar](#)] [[Publisher Link](#)]
- [2] Mahbub Ul Islam Khan et al., "Securing Electric Vehicle Performance: Machine Learning-Driven Fault Detection and Classification," *IEEE Access*, vol. 12, pp. 71566-71584, 2024. [[CrossRef](#)] [[Google Scholar](#)] [[Publisher Link](#)]
- [3] S. Aslam et al., "Hamiltonian Deep Neural Network Technique Optimized with Lyrebird Optimization Algorithm for Detecting and Classifying Power Quality Disturbances in PV Combined DC Microgrids System," *Environment, Development and Sustainability*, 2025. [[CrossRef](#)] [[Google Scholar](#)] [[Publisher Link](#)]
- [4] Mohammed H. Ibrahim, Ebrahim A. Badran, and Mansour H. Abdel-Rahman, "Detect, Classify, and Locate Faults in DC Microgrids Based on Support Vector Machines and Bagged Trees in the Machine Learning Approach," *IEEE Access*, vol. 12, pp. 139199-139224, 2024. [[CrossRef](#)] [[Google Scholar](#)] [[Publisher Link](#)]
- [5] K. Mohana Sundaram et al., "Deep Learning for Fault Diagnostics in Bearings, Insulators, PV Panels, Power Lines, and Electric Vehicle Applications the State-of-the-Art Approaches," *IEEE Access*, vol. 9, pp. 41246-41260, 2021. [[CrossRef](#)] [[Google Scholar](#)] [[Publisher Link](#)]
- [6] Nien-Che Yang, and Mohd Faizan, "Long Short-Term Memory-Based Feedforward Neural Network Algorithm for Photovoltaic Fault Detection under Irradiance Conditions," *IEEE Transactions on Instrumentation and Measurement*, vol. 73, pp. 1-11, 2024. [[CrossRef](#)] [[Google Scholar](#)] [[Publisher Link](#)]
- [7] Mauricio Lavador-Osorio et al., "An Enhanced Frequency Analysis and Machine Learning Based Approach for Open Circuit Failures in PV Systems," *IEEE Access*, vol. 12, pp. 96342-96357, 2024. [[CrossRef](#)] [[Google Scholar](#)] [[Publisher Link](#)]
- [8] Ehtisham Lodhi et al., "A Novel Deep Stack-Based Ensemble Learning Approach for Fault Detection and Classification in Photovoltaic Arrays," *Remote Sensing*, vol. 15, no. 5, pp. 1-26, 2023. [[CrossRef](#)] [[Google Scholar](#)] [[Publisher Link](#)]
- [9] Yue Zhang et al., "Data-Driven Day-Ahead PV Estimation Using Autoencoder-LSTM and Persistence Model," *IEEE Transactions on Industry Applications*, vol. 56, no. 6, pp. 7185-7192, 2020. [[CrossRef](#)] [[Google Scholar](#)] [[Publisher Link](#)]
- [10] Montaser Abdelsattar et al., "Assessing Machine Learning Approaches for Photovoltaic Energy Prediction in Sustainable Energy Systems," *IEEE Access*, vol. 12, pp. 107599-107615, 2024. [[CrossRef](#)] [[Google Scholar](#)] [[Publisher Link](#)]
- [11] R. Sundaramoorthi, and S. Chitraselvi, "Integration of Renewable Resources in Electric Vehicle Charging Management Systems Using Deep Learning for Monitoring and Optimization," *Iranian Journal of Science and Technology, Transactions of Electrical Engineering*, vol. 49, pp. 313-335, 2025. [[CrossRef](#)] [[Google Scholar](#)] [[Publisher Link](#)]
- [12] Debabrata Mazumdar et al., "An Enhanced MPPT Approach Based on CUSA for Grid-Integrated Hybrid Electric Vehicle Charging Station," *International Journal of Energy Research*, vol. 2024, no. 1, pp. 1-14, 2024. [[CrossRef](#)] [[Google Scholar](#)] [[Publisher Link](#)]
- [13] Ali Teta et al., "Fault Detection and Diagnosis of Grid-Connected Photovoltaic Systems Using Energy Valley Optimizer Based Lightweight CNN and Wavelet Transform," *Scientific Reports*, vol. 14, no. 1, pp. 1-22, 2024. [[CrossRef](#)] [[Google Scholar](#)] [[Publisher Link](#)]
- [14] Chavan Vinaya Chandrakant, and Suresh Mikkili, "A Typical Review on Static Reconfiguration Strategies in Photovoltaic Array under Non-Uniform Shading Conditions," *CSEE Journal of Power and Energy Systems*, vol. 9, no. 6, pp. 2018-2039, 2023. [[CrossRef](#)] [[Google Scholar](#)] [[Publisher Link](#)]
- [15] Dhritiman Adhya, Soumesh Chatterjee, and Ajoy Kumar Chakraborty, "Performance Assessment of Selective Machine Learning Techniques for Improved PV Array Fault Diagnosis," *Sustainable Energy, Grids and Networks*, vol. 29, 2022. [[CrossRef](#)] [[Google Scholar](#)] [[Publisher Link](#)]
- [16] Ahmed Faris Amiri et al., "Faults Detection and Diagnosis of PV Systems Based on Machine Learning Approach Using Random Forest Classifier," *Energy Conversion and Management*, vol. 301, 2024. [[CrossRef](#)] [[Google Scholar](#)] [[Publisher Link](#)]
- [17] Xiaotian Zhang et al., "Artificial Intelligence Technique-Based EV Powertrain Condition Monitoring and Fault Diagnosis: A Review," *IEEE Sensors Journal*, vol. 23, no. 15, pp. 16481-16500, 2023. [[CrossRef](#)] [[Google Scholar](#)] [[Publisher Link](#)]
- [18] Hicham El Hadraoui et al., "Toward an Intelligent Diagnosis and Prognostic Health Management System for Autonomous Electric Vehicle Powertrains: A Novel Distributed Intelligent Digital Twin-Based Architecture," *IEEE Access*, vol. 12, pp. 110729-110761, 2024. [[CrossRef](#)] [[Google Scholar](#)] [[Publisher Link](#)]
- [19] Ahmed Althobaiti et al., "Intelligent Data Science Enabled Reactive Power Optimization of a Distribution System," *Sustainable Computing: Informatics and Systems*, vol. 35, 2022. [[CrossRef](#)] [[Google Scholar](#)] [[Publisher Link](#)]
- [20] P. Balakumar, Senthil Kumar Ramu, and T. Vinopraha, "Optimizing Electric Vehicle Charging in Distribution Networks: A Dynamic Pricing Approach Using Internet of Things and Bi-Directional LSTM Model," *Energy*, vol. 294, 2024. [[CrossRef](#)] [[Google Scholar](#)] [[Publisher Link](#)]
- [21] Abdullah M. Shaheen et al., "A Forensic-Based Investigation Algorithm for Parameter Extraction of Solar Cell Models," *IEEE Access*, vol. 9, pp. 1-20, 2020. [[CrossRef](#)] [[Google Scholar](#)] [[Publisher Link](#)]
- [22] M. Aishwarya, and R.M. Brisilla, "Design and Fault Diagnosis of Induction Motor Using ML-Based Algorithms for EV Application," *IEEE Access*, vol. 11, pp. 34186-34197, 2023. [[CrossRef](#)] [[Google Scholar](#)] [[Publisher Link](#)]
- [23] Anil Kumar et al., "Novel Convolutional Neural Network (NCNN) for the Diagnosis of Bearing Defects in Rotary Machinery," *IEEE Transactions on Instrumentation and Measurement*, vol. 70, pp. 1-10, 2021. [[CrossRef](#)] [[Google Scholar](#)] [[Publisher Link](#)]

- [24] Mohammad Noroozi et al., "Golden Search Optimization Algorithm," *IEEE Access*, vol. 10, pp. 37515-37532, 2022. [[CrossRef](#)] [[Google Scholar](#)] [[Publisher Link](#)]
- [25] GPVS-Faults-Detection, Github. [Online]. Available: <https://github.com/anila14-del/GPVS-Faults-Detection>